Synthesis and characterisation of quantum dots coupled to mycolic acids as a water-soluble fluorescent probe for potential lateral flow detection of antibodies and diagnosis of tuberculosis

Kapambwe P. Kabwe,[1] Sifiso A. Nsibande,[1] Yolandy Lemmer,[2] Lynne A. Pilcher,[1] Patricia B.C. Forbes[1]*

[1] Department of Chemistry, Faculty of Natural and Agricultural Sciences, University of Pretoria, Pretoria, South Africa.

[2] CSIR-Next Generation Health, Pretoria, 0001, South Africa

*Corresponding author: patricia.forbes@up.ac.za

Abstract

This work explores the potential use of cadmium-based quantum dots (QDs) coupled to mycolic acids (MAs) as a fluorescent probe to detect anti-MA antibodies which are biomarkers for tuberculosis (TB). The use of free MAs as antigens for the serodiagnosis of TB is known but has not been developed into a point of care test. This study focuses on the synthesis, solubility, and lateral flow of QDs coupled to MAs. Water-soluble CdSe/ZnS QDs capped with L-cysteine were synthesised and covalently coupled to MAs via amide linkages to form a water-soluble fluorescent probe: MA-CdSe/ZnS QDs. The MA-CdSe/ZnS QDs showed broad absorption bands and coupling, confirmed by the presence of amide bonds in the FT-IR spectrum, resulted in a blue shift in fluorescence. Powder XRD revealed a shift and increase in the number of peaks for MA-CdSe/ZnS QDs relative to the L-cys-CdSe/ZnS QDs, suggesting that coupling changed the crystal structure. The average particle size of MA-CdSe/ZnS QDs was ~3.0 nm. Visual paper-based lateral flow of MA-CdSe/ZnS QDs was achieved on strips of nitrocellulose membrane with both water and membrane blocking solution eluents. The highly fluorescent MA-CdSe/ZnS QDs showed good water solubility and lateral flow, which are important properties for fluorescence sensing applications.

Keywords: fluorescence; quantum dots; mycolic acids; biomarkers; tuberculosis.

1. Introduction

Tuberculosis is a global health problem due to co-infection with HIV and the development of drug-resistant strains. It is a chronic pulmonary disease caused by the *mycobacterium tuberculosis* (M.tb) bacterium. [1] M.tb is transmitted through sputum droplets released through speaking, coughing, and sneezing, and the bacterium replicates every 18-72 hrs. [2] M.tb can be taken up by alveolar macrophages and forms a protective granuloma to sustain a long-term infection. [3] TB is a serious challenge in developing countries as well as an increasing scourge in many developed areas of the world. The World Health Organization (WHO) Global Tuberculosis Series 2020 reported that 10.0 million new cases of TB in 2019, and 1.5 million TB deaths among HIV-positive people were recorded. [4]

Despite considerable improvement in the diagnosis of TB over the past years, a simple and effective method for the early detection of TB at the point of care is not yet available. [5] As a result, the start of treatment could be delayed, allowing the disease to spread. Some of the current challenges in TB detection and diagnosis include inaccurate results, low sensitivity and time taken between detection and the correct diagnosis. The more accurate TB tests that are currently used, such as chest X-rays, are expensive particularly for developing countries. [5] The occurrence of TB and the increased risk of TB in HIV infected persons have boosted the need for rapid, inexpensive, and accurate methods for the detection and diagnosis of TB.

Sputum analysis research has been conducted to determine the presence of live M.tb in different ways and is used in TB detection and diagnosis. This technique is very sensitive with a low detection limit for M.tb, but it takes 6-8 weeks to give a diagnosis. Because of this delayed diagnosis, patient care and TB control can be affected as it gives enough time for the spread of the infection. The other limitation is that HIV infected patients do not produce the desired quality sputum sample for TB detection due to their weak immune systems. [6] The lipoarabinomannan (LAM) urine dipstick test is also used to diagnose TB. [7] The use of this test has gained popularity as it is simple, easy to use and is more sensitive than the sputum test for people with HIV. Although the LAM test has worked well for people with very low CD4 counts, false negatives are common and other confirmatory TB tests need to be conducted. [7, 8] The colloidal gold test is another method used to detect antibodies to TB in blood serum. This involves marking of antigens on gold nanoparticles to establish an antigen colloidal gold immunochromatographic assay. [9] In this test, the antibodies from TB patients bind to the antigens marked on the colloidal gold nanoparticles to form antibody-antigen gold nanoparticle

complexes. These complexes then produce a colour to indicate that the antibodies have been detected. The method works well because it is sensitive and specific, but the detection process is time-consuming as it involves a longer period of incubation, and the potential toxicity of gold nanoparticles limits its application. [9, 10] Therefore, a more simplified and user-friendly test is required for TB antibody detection.

Mycolic acids (MAs) are the most abundant lipids found in the cell walls of *mycobacterium tuberculosis.* [11] These long chain waxes with chain lengths of 60 to 90 carbons form a hydrophobic shell around the organism, protecting it from attack by oxygen radicals, cationic proteins, and lysozymes that are found in the phagocytic granule. [12] It has been determined that MAs are antigenic, eliciting an immune response even in immune compromised HIV positive individuals. [13] The antibodies to MAs can be used as surrogate markers for active TB. However, the poor solubility of MAs in most solvents (they are only soluble in chloroform and hexane) presents the biggest challenge in their application. [14] The Mycolic Acid Real Time Inhibition (MARTI) test that has good accuracy and sensitivity in both HIV− and HIV+ patients has been developed based on the detection of anti-MA antibodies in human serum using surface plasmon resonance, [15] or electrochemical impedance spectroscopy (EIS). [16] The MARTI EIS technology has been adapted to the use of screen-printed electrodes with the aim of developing a reliable point of care diagnostic, [17] but the technology is proving challenging.

Cadmium-based quantum dots (QDs) are nanocrystals with the size range between 1-10 nm. [18] Different cadmium-based QDs have been produced over the past decades and have been applied in various fields because of their electronic and optical properties including; high surface to volume ratio, size-tuneable band gap energy, narrow emission spectra and broad absorption spectra. Cadmium-based QDs also have high fluorescence quantum yields and higher resistance to photo-initiated degradation as compared to organic fluorophores. The functional groups bound on the surface of QDs define their solubility and strongly influence their physical and photophysical properties. The shell protects material inside the core against photo-oxidation degradation and provides another way for surface functionalisation with different ligands. Because of these properties, cadmium based QDs have been used extensively in scientific and technological applications that rely on achieving spectral purity at optimum optical flux such as chemical/biological sensing, optoelectronic devices, molecular biology, bioimaging, and photochemistry. [19-21]

The paper-based lateral-flow assay is a simple, low-cost test that is used to detect the presence of a target analyte; usually an antibody in a solution. The assay is used for biological applications including rapid detection of diseases based on the biochemical interactions, such as antigen-antibody interaction without much sample processing, making it ideal for a point of care diagnostic tool. [22] The lateral flow device consists of four sections mounted on the cardboard support for easy handling and stability. The sample pad is the first section where the sample is introduced. The conjugation pad is the region where the biomarker antibodies in the sample and pre-loaded labelled antigen combine to form an immune complex. The immune complex flows through the nitrocellulose membrane towards the test line for further antigen-antibody interaction between the immune complex and immobilized antibody. Attached at the end of the strip is an absorbent pad used as a reservoir for waste and preventing the backflow of the liquid. [23, 24] To develop such a test based on the MA-anti-MA (antigen-antibody) interaction one could make use of anti-MA antibodies that have been developed, [25] but it would be necessary to add a fluorescent tag to the MAs in order to visualise the antibody-antigen-antibody aggregate and it would be necessary to solubilize the hydrophobic MAs in order for it to interact with the aqueous serum.

To the best of our knowledge, the use of MAs coupled to water-soluble CdSe/ZnS QDs capped with L-cysteine has not been previously reported as a water-soluble fluorescent tuberculosis probe. It is anticipated that the coupling of MAs to water-soluble fluorescent CdSe/ZnS QDs would improve its solubility and open doors for it to be used as a fluorescent probe that can be used for detection of anti-MA antibodies in serum for the diagnosis of TB. Here we report on the coupling of MAs to water-soluble core/shell CdSe/ZnS QDs capped with L-cysteine for the first time, and we show that this improves the solubility of MAs. We show for the first time the visual paper-based lateral flow of MA-CdSe/ZnS QDs through a nitrocellulose membrane. This work demonstrates the potential application of MA-CdSe/ZnS QDs as a fluorescent tuberculosis biomarker.

2. Experimental

2.1 Materials and reagents

Cadmium oxide (CdO, 99.5%), oleic acid (OA, 90%), octadecene (ODE, 90%), selenium (Se, 99%), trioctylphosphine oxide (TOPO,90%), sulphur (S, 99.5%), zinc oxide (ZnO, 99%) L-cysteine (96%), L-cystine (98 %), 1-ethyl-3-(3-dimethylaminopropyl) carbodiimide (EDC, 98%), n-hydroxysuccinimide (NHS, 98%), dicyclohexycarbodiimide (DCC, 98%), thionyl

chloride ($SOCl_2$, 98%), oxalyl chloride ($(COCl)_2$, 98%) and mycolic acid (MA, 98%) were purchased from Sigma-Aldrich (Germany) and were used without further purification. The solvents: methanol (99%), acetone (99.5%), dichloromethane (DCM, 99.8%), tetrahydrofuran (THF) dimethylformamide (DMF, 99%), ethyl acetate (98%), dimethyl sulfoxide (DMSO, 99%), and chloroform ($CHCl_3$, 99%) were purchased from Associated Chemical Enterprises, South Africa and were also used as received. Other solid materials that were purchased from Associated Chemical Enterprises include sodium chloride (99%), potassium chloride (99%), disodium phosphate (Na_2HPO_4, 98%), potassium dihydrogen phosphate (KH_2PO_4, 98%), Potassium hydroxide (85%), sodium sulphate (99%), sodium hydrogen carbonate (98%) and sodium hydroxide (97%). Stearic acid (99%), glycine (99%), hydrochloric acid (98%), pyridine (99.5%), and triethylamine (TEA, 99%) were purchased from Radchem Laboratory Chemicals and Consumables (South Africa). Argon was supplied by African Oxygen Limited (Afrox, South Africa) while deionised water was obtained from an in-house laboratory water purification system (Drawell Scientific Instrument Co, Ltd, USA). Macherey-Nagel Whatman filter papers (MN 615 diameter 125 mm) were purchased from Altmann Analytik GmbH & Co. KG (Germany).

2.2 Equipment

The ground state electronic absorption of CdSe/ZnS QDs, L-cys-CdSe/ZnS QDs, MA-CdSe/ZnS QDs and 4MA-CdSe/ZnS QDs were recorded on a Cary Eclipse UV-visible spectrophotometer (Varian Pty Ltd, Australia) with the wavelength range 200 to 800 nm. Fluorescence emission results were achieved using a Horiba Jobin Yvon Fluoromax-4 spectrofluorometer (Horiba Instruments Inc., Edison, NJ, USA). Infra-red spectra in the range of 4000-400 cm^{-1} were recorded on an Alpha (II) Bruker spectrometer (Bruker Optik GMBh, Ettlingen, Germany), equipped with Opus open-source software. The size and morphology of the materials were studied with the transmission electron microscope (TEM) (JEOL JEM 2100F, JOEL Ltd, Tokyo, Japan) with emission at 200 kV, and particle size distribution was determined with ImageJ software. Powder X-ray diffraction patterns were recorded on a Bruker D2 phaser (Bruker AXS GmbH, Karlsruhe, German) using Cu (Kα) radiation (wavelength of the X-ray source is 1.54184Å). ^{1}H and ^{13}C NMR spectra were obtained using a Brucker Avance III 300MHz NMR spectrometer (Bruker Biospin GmbH, Rheinstetten, Germany) in dimethyl sulfoxide DMSO.

2.3 Synthesis

2.3.1 Synthesis of water-soluble core/shell CdSe/ZnS quantum dots capped with L-cysteine (L-cys-CdSe/ZnS QDs)

Before the CdSe/ZnS quantum dots were synthesized, three different precursors, namely selenium, sulphur and zinc precursors were prepared as sources of Se, S, and Zn respectively following a previously reported procedure, [26] with some modifications. For the selenium precursor, 1.54 g of trioctylphosphine oxide (TOPO), which serves as a surfactant was dissolved in 20 ml of octadec-1-ene (ODE) and heated to ensure complete dissolution. After that, 0.24 g of Se powder was added and the mixture was sonicated for 10 min followed by stirring at room temperature overnight at 750 rpm. The sulphur precursor was prepared by dissolving 1.54 g of TOPO in 24 ml of ODE and 16 ml of oleic acid (OA). The mixture was heated for a few minutes to ensure complete dissolution. 0.13 g of sulphur was added, and the mixture was heated for a few minutes and later sonicated for 15-20 min to speed up the dissolution of the sulphur. The solution was kept stirring overnight at room temperature. The zinc precursor was prepared by adding 0.30 g of zinc oxide (ZnO) to the solution of 24 ml of ODE and 15 ml of OA at room temperature and stirred. The mixture was sonicated for 15-20 min to ensure complete dissolution and was kept stirring at room temperature overnight at 750 rpm.

After preparation of the precursors, core/shell CdSe/ZnS QDs capped with L-cysteine were synthesized according to a previously reported method, [26, 27] with minor modifications. Briefly, 1.00 g cadmium oxide (CdO) as a source of Cd was added into a solution of 38 ml ODE and 23 ml OA. The reaction mixture was rapidly stirred for 30 min at 280 ^{o}C under an inert environment (using argon) to form a colourless solution of Cd-ODE-OA. To this solution, 15 ml of the selenium precursor was added to allow for nucleation and growth of the CdSe core. After 5 min, 15 ml of Zn and S precursors were added to the solution to passivate the core with a ZnS shell and reduce surface defects. The shell was allowed to grow at a reduced temperature of 200 ^{O}C for 40 min and the colour changed from yellow to orange to red before the reaction was stopped. To obtain hydrophobic CdSe/ZnS QDs, methanol was added, and the mixture was allowed to stand overnight. The hydrophobic core/shell CdSe/ZnS QDs were then purified by washing with methanol and acetone with centrifuging at 6000 rpm.

The hydrophobic CdSe/ZnS QDs were made water-soluble by the addition of hydrophilic L-cysteine as follows: in 33 ml of methanol, 2.50 g of KOH and 1.70 g of L-cysteine were added

and dissolved via ultra-sonication to form a solution of the methanolic-KOH-L-cysteine. After 10 min of ultra-sonication, hydrophobic CdSe/ZnS QDs dissolved in chloroform and deionised water was added until the mixture became clear. The solution was stirred for a few minutes and allowed to stand overnight at room temperature to allow for ligand exchange (**Fig. 1**). The resulting water-soluble CdSe/ZnS QDs capped with L-cysteine (denoted as L-cys-CdSe/ZnS QDs) were purified by washing with acetone, chloroform, then with a mixture of acetone and chloroform, chloroform alone and finally with acetone through centrifugation at a speed of 6000 rpm.

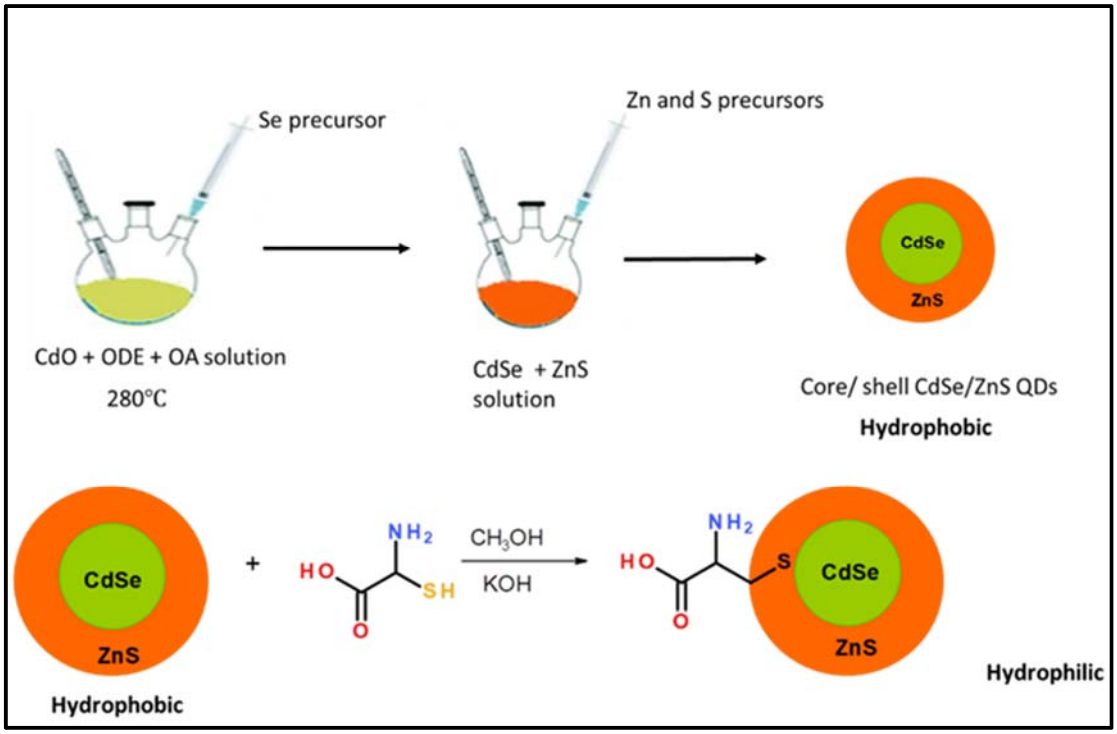

Fig. 1: Schematic diagram illustrating the synthesis of water-soluble core/shell CdSe/ZnS QDs capped with L-cysteine.

2.3.2 Development of coupling reaction method

Several approaches had to be explored for the coupling of mycolic acids (MAs) to quantum dots (QDs). MAs are hydrophobic and soluble only in chloroform and hexane, whereas the QDs capped with L-cysteine are water soluble. This posed a challenge to synthesis: how to bring the compounds together for covalent coupling. Due to the high cost of MA, we set out to develop appropriate coupling chemistry using model compounds. Stearic acid was chosen as the model for MA due to its carboxylic acid group and 18-carbon hydrophobic chain, giving it similar solubility properties to MA. Glycine and the dipeptide cystine were selected as possible

models for the surface capping on the QDs to allow for structural characterization of the amide products by NMR analysis. Many different synthetic approaches have been developed for the formation of amide bonds, such as coupling acid chlorides to amines and carbodiimide chemistry. Attempts to use carbodiimide chemistry in the reaction of stearic acid with dipeptide l-cystine and stearic acid with glycine using 1-ethyl-3-(3-dimethylaminopropyl) carbodiimide (EDC) and N-hydroxysuccinimide (NHS) in acetone/water or dicyclohexylcarbodiimide (DCC) and NHS in water/ tetrahydrofuran (THF) were not successful. Stearic acid was successfully converted to stearic acid chloride using either thionyl chloride or oxalyl chloride in dichloromethane DCM, but the subsequent reaction with glycine refluxing in anhydrous dimethylformamide (DMF) did not yield the amide. After a number of attempts, we achieved the coupling of the stearic acid chloride and glycine in dry chloroform or DCM using DMF as a catalyst. The coupling yield was improved by replacing DMF with triethylamine and adding a catalytic amount of pyridine. The structure of the stearoyl-glycine amide was confirmed using ^{1}H and ^{13}C NMR and FT-IR analysis.

These reaction conditions were successfully employed for the coupling of stearic acid to L-cys-CdSe/ZnS QDs to form stearoyl-CdSe/ZnS QDs amide. The formation of stearoyl-CdSe/ZnS QDs amide was confirmed by FT-IR to be similar to that of the stearic -glycine amide. A blue shift in the fluorescence emission wavelengths indicated a change in the surface structure of the QDs, and evidence of the successful coupling of stearic acid to the L-cys-CdSe/ZnS QDs.

2.3.3 Coupling of stearic acid to glycine

In 10 ml of dry DCM, stearic acid (1.44 g) and 1 drop of DMF were mixed. The reaction mixture was stirred at room temperature for 5 min, then $(COCl)_2$ (1.00 ml) was added to the mixture. The mixture was left stirring at 750 rpm for 12 hr at room temperature. The excess solvent was removed using a rotary evaporator to obtain a yellow oil product called stearoyl-chloride (S-Cl), which was used directly in the next step without purification.

To couple S-Cl to glycine, 0.78 g of glycine was dissolved in 16.2 ml of dry DCM with continuous stirring while purging with argon at 750 rpm. Two drops of pyridine were added to the reaction mixture as a catalyst. The mixture was stirred in the bath of acetone and dry ice to a temperate between -15 ^{0}C - 0 ^{0}C. 1.2 ml of stearoyl chloride was added dropwise while cooling the mixture. Immediately after all the stearoyl chloride was added, trimethylamine was added as a base. The mixture was kept stirring at 750 rpm for 12 hr at room temperature. The

reaction mixture was then filtered using Macherey-Nagel Whatman filter paper (MN 615 diameter 125 mm) to remove excess stearoyl chloride. The filtrate was dried using a rotary evaporator to obtain orange crystals of stearoyl glycine amide **(**S-G), as illustrated in **Fig 2**.

Results; 1H NMR: δH (300 MHz; DMSO), 0.89 (3H, t, CH_3), 1.31 (30 H, m, 15 x CH_2), 2.16 (2H, t, CH_2), 3.86 (2H, d, CH_2), 8.11 (1H, t, NH), 10.07 (1H, s, COOH), 13C NMR: δC (300 MHz; DMSO), 15.13, 23.14, 25.31, 30.56, 32.63, 173.61,174.56. IR [(KBr) vmax, cm $^{-1}$)]: (-C=O = 1700), (-C-H =3000), (-N-H = 3320), (-N-C=O =2500-2650).

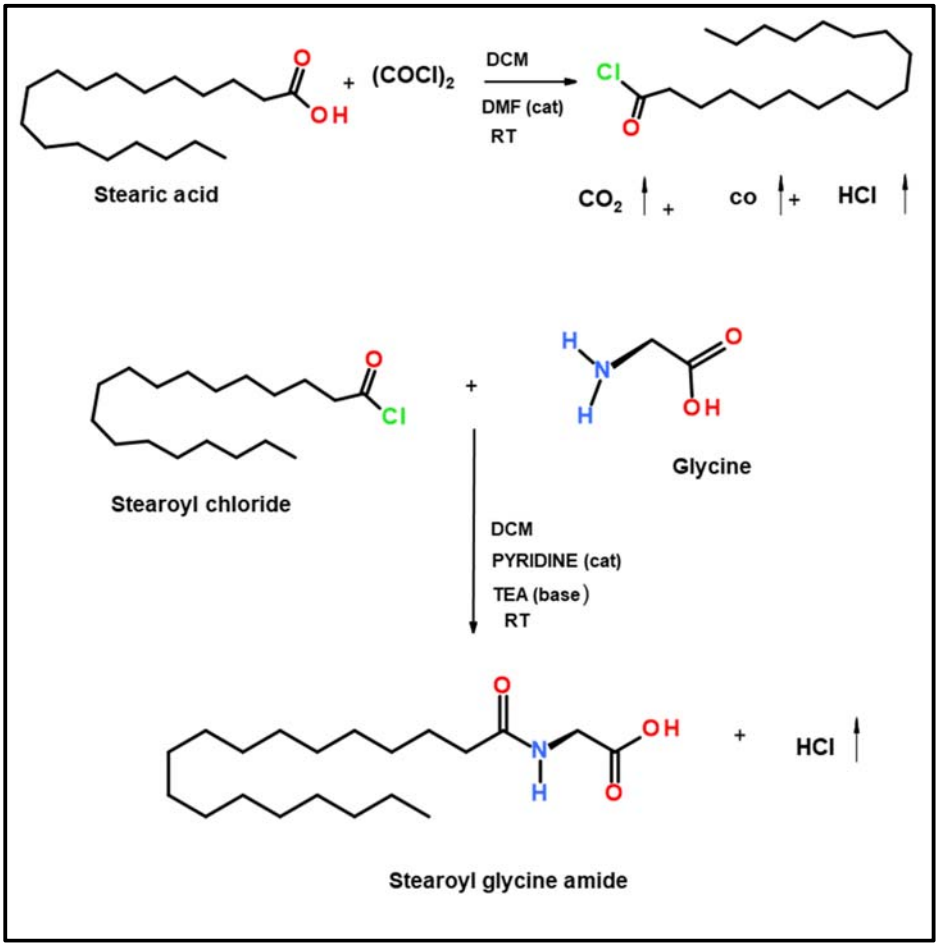

Fig 2: Schematic illustration of the covalent coupling of stearic acid to glycine to form stearoyl glycine amide.

2.3.4 Covalent coupling of mycolic acid to water-soluble core/shell CdSe/ZnS QDs capped with L-cysteine

In a 50 ml round bottomed flask, 3 ml of dry $CHCl_3$, 1.00 mg of MA and 1 drop of DMF were mixed. The reaction mixture was stirred at room temperature for 5 min and then 0.50 ml of

oxalyl chloride $(COCl)_2$ was added to the reaction mixture which was kept stirring at room temperature for 12 hrs at 750 rpm. After this, excess solvent was removed using a rotary evaporator to obtain mycolic acid chloride (MA-Cl) as a yellow oily product. MA-Cl was used directly in the next step without further purification.

To couple MA-Cl to hydrophilic CdSe/ZnS QDs, 0.06 g of the hydrophilic QDs were suspended in 3 ml of dry DCM in a 100 ml round bottomed flask and the suspension was purged with argon while stirring at 750 rpm for 5 min. Two drops of pyridine were added to the reaction mixture as a catalyst to replace chloride with pyridine. The mixture was placed in a bath of acetone and dry ice while stirring at a temperature between -15 ^{o}C and 0 ^{o}C. MA-Cl was added drop by drop while cooling the mixture. Immediately after MA-Cl, five drops of triethylamine (TEA) were added as a base. The reaction mixture was left stirring at room temperature for 12 hrs at 750 rpm (**Fig. 3**). The reaction mixture was then filtered (Macherey-Nagel Whatman filter paper MN 615 diameter 125 mm) to remove excess L-cys-CdSe/ZnS-QDs. The filtrate was concentrated in vacuo to obtain orange crystals of mycolic acid-CdSe/ZnS QDs capped with L-cysteine denoted as MA-CdSe/ZnS QDs.

Covalent coupling of mycolic acid to water-soluble core/shell CdSe/ZnS QDs capped with L-cysteine was repeated using 4.00 mg of MAs, 9 ml of chloroform, and 1.5 ml of oxalyl chloride, following the same procedure as above. This was done to increase the amount of MAs on the coupled material. The new product was denoted as 4MA-CdSe/ZnS QDs.

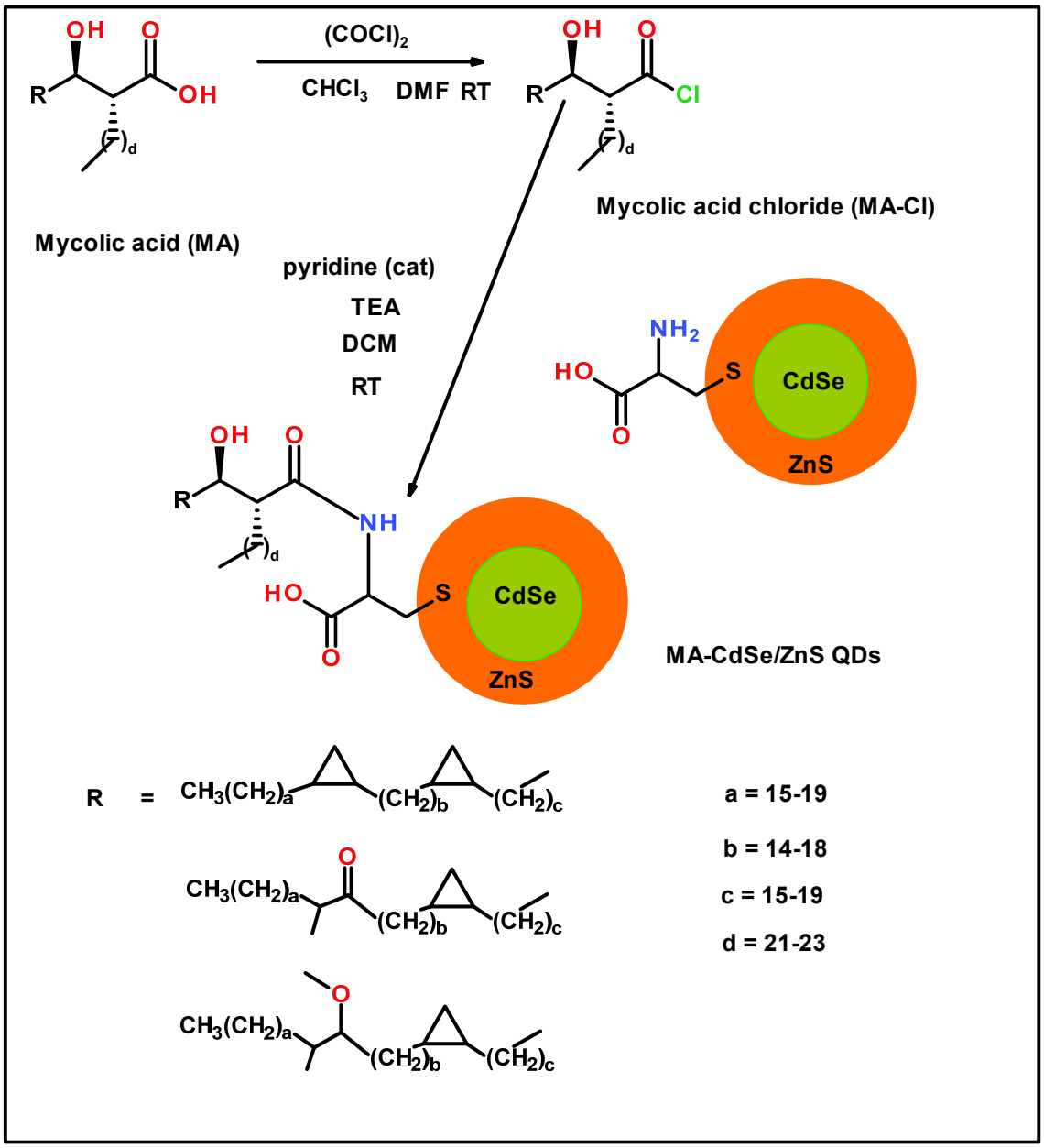

Fig. 3: Schematic illustration of the covalent coupling of water-soluble CdSe/ZnS QDs capped with L-cysteine to MAs to form a water-soluble fluorescent probe for TB biomarkers: MA-CdSe/ZnS QDs. As natural MA isolated from *Mycobacterium tuberculosis* bovine strain was used, R represents a range of similar side chains of which the most common are shown.

2.4 Determination of fluorescence quantum efficiency (QE)

The fluorescence quantum efficiency of quantum dots is measured in relation to fluorescence quantum yields (Φ_f) as previously reported.[28] In this study, the fluorescence quantum efficiency was measured by determining the fluorescence quantum yields of the QDs using Equation 1, which compares the fluorescence intensities of the sample (I_{sam}) to Rhodamine 6G

as a reference standard in ethanol (I_{std}) with respective absorbances of A_{sam} and A_{std}. The fluorescence quantum yield of Rhodamine 6G was used as a standard denoted as Φ_{std}. The refractive index of water for L-cys-CdSe/ZnS QDs (n_{sam}), chloroform for CdSe/ZnS QDs (n_{sam}) and ethanol for Rhodamine 6G were used as standards (n_{std}), respectively.[29] The excitation wavelength (390 nm) was the same for all the measurements, while the absorbance values were kept at less than 0.05 to reduce inner filter effects.

$$\Phi_f = \Phi_{std} * \frac{I_{sam} * A_{std} * n^2{}_{sam}}{I_{std} * A_{sam} * n^2{}_{std}}$$

Equation 1

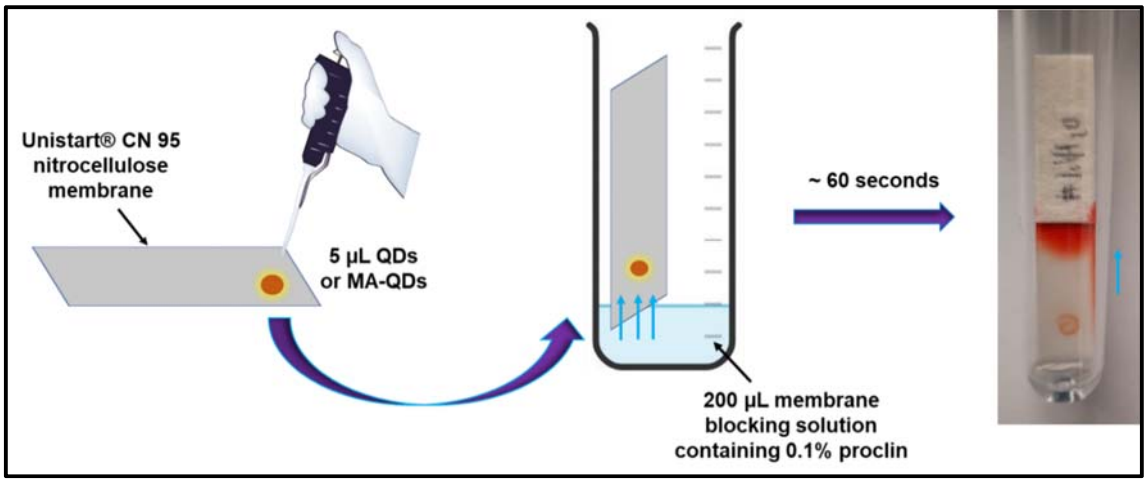

Fig. 4: Schematic illustration of the procedure for the paper-based lateral flow test for L-cys-CdSe/ZnS QDs, MA-CdSe/ZnS QDs and 4MA-CdSe/ZnS QDs with membrane blocking solution as an eluent.

2.5 Paper-based lateral flow of L-cys-CdSe/ZnS QDs, MA-CdSe/ZnS QDs and 4MA-CdSe/ZnS QDs

In small vials, 0.01 mg of L-cys-CdSe/ZnS QDs, MA-CdSe/ZnS QDs and 4MA-CdSe/ZnS QDs respectively were each dissolved in 100 µL of deionized water to form 0.1 g/L solutions. Two experiments were done in triplicate as follows: in the first experiment, water was used as an eluent with each of the materials (fluorophores) to determine if their flow on the strip of nitrocellulose membrane in water was visually noticeable. To do this, 5 µL aliquot of each of the 0.1 g/L solutions of the fluorophores was spotted onto the strips of nitrocellulose membrane using a 5 µL Eppendorf pipette. The strips were then placed vertically in individual test tubes containing 200 µL of water as an eluent as shown in **Fig. 4**. In the second experiment, a membrane blocking solution containing 0.1% proclin was used as an eluent instead of water

with each of the fluorophores, following the same procedure. The resulting nitrocellulose membrane strips were then scanned using a light HP Scanjet 2400 flatbed scanner for visual analysis.

3. Results and Discussion

3.1 Absorption properties of CdSe/ZnS QDs, L-cys-CdSe/ZnS QDs, MA-CdSe/ZnS QDs and 4MA-CdSe/ZnS QDs

The optical properties of CdSe/ZnS QDs, **L-cys-**CdSe/ZnS QDs**,** MA-CdSe/ZnS QDs and 4MA-CdSe/ZnS QDs were investigated using UV-vis spectroscopy (**Fig. 5)**. The UV-vis spectra for all QD products show broad absorption bands from 200 to 300 nm which is a useful property, as it allows for varying excitation wavelengths to be employed in fluorescence sensing applications. These results show that the amount of MAs does not significantly affect the absorption bands of coupled material, although 4MA-CdSe/ZnS QDs had a strong absorption band in the region 220 to 260 nm.

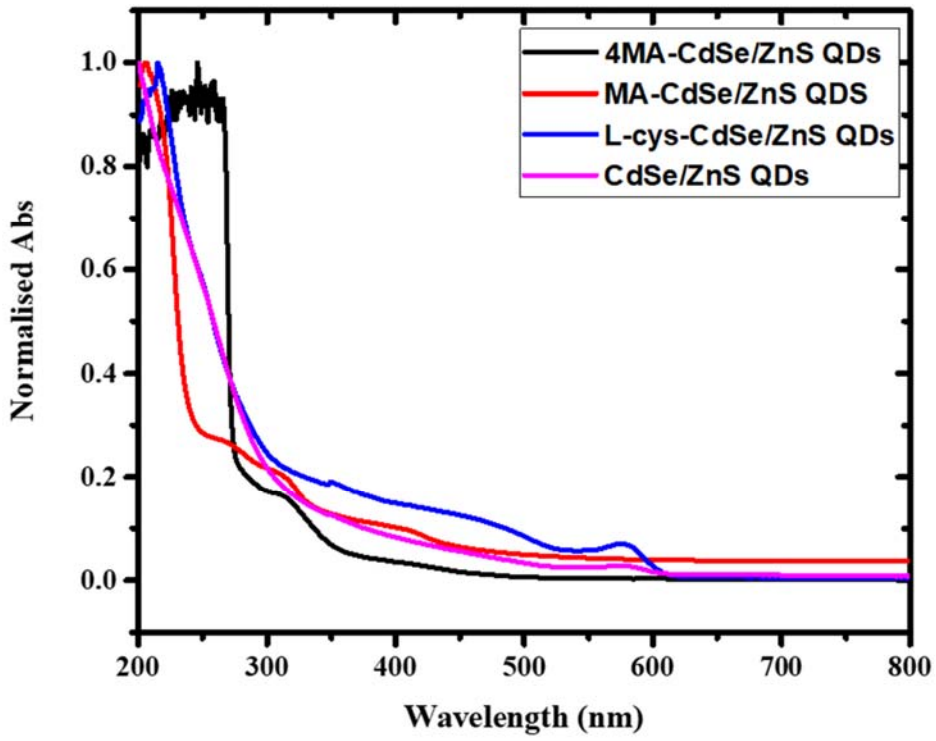

Fig. 5: Normalised UV-vis absorption spectra of CdSe/ZnS QDs (dissolved in chloroform), **L-cys-**CdSe/ZnS QDs, MA-CdSe/ZnS QDs and 4MA-CdSe/ZnS QDs dissolved in water.

3.2 Effect of excitation wavelength on fluorescence emission spectra of L-cys-CdSe/ZnS QDs, MA-CdSe/ZnS QDs and 4MA-CdSe/ZnS QDs

The effect of excitation wavelength on the fluorescence emission wavelengths of L-cys-CdSe/ZnS QDs, MA-CdSe/ZnS QDs and 4MA-CdSe/ZnS QDs were investigated. **Fig. 6** shows that the excitation wavelength that gave the highest emission wavelength intensity for L-cys-CdSe/ZnS QDs was 400 nm while for the MA-CdSe/ZnS QDs and for 4MA-CdSe/ZnS QDs it was 380 nm. It was noticed that changing the excitation wavelength did not affect the emission wavelength of L-cys-CdSe/ZnS QDs, but an increase in emission wavelength (red-shifting) was observed for MA-CdSe/ZnS QDs and 4MA-CdSe/ZnS QDs when the excitation wavelength was increased. The fluorescence emission intensity of L-cys-CdSe/ZnS QDs initially increased to the maximum and thereafter decreased while increasing the excitation wavelength (**Fig. 6A and 6D**). For MA-CdSe/ZnS QDs and 4MA-CdSe/ZnS QDs, the fluorescence emission intensity continued to decrease while the excitation wavelength increased (**Fig. 6B, 6C, and 6D).**

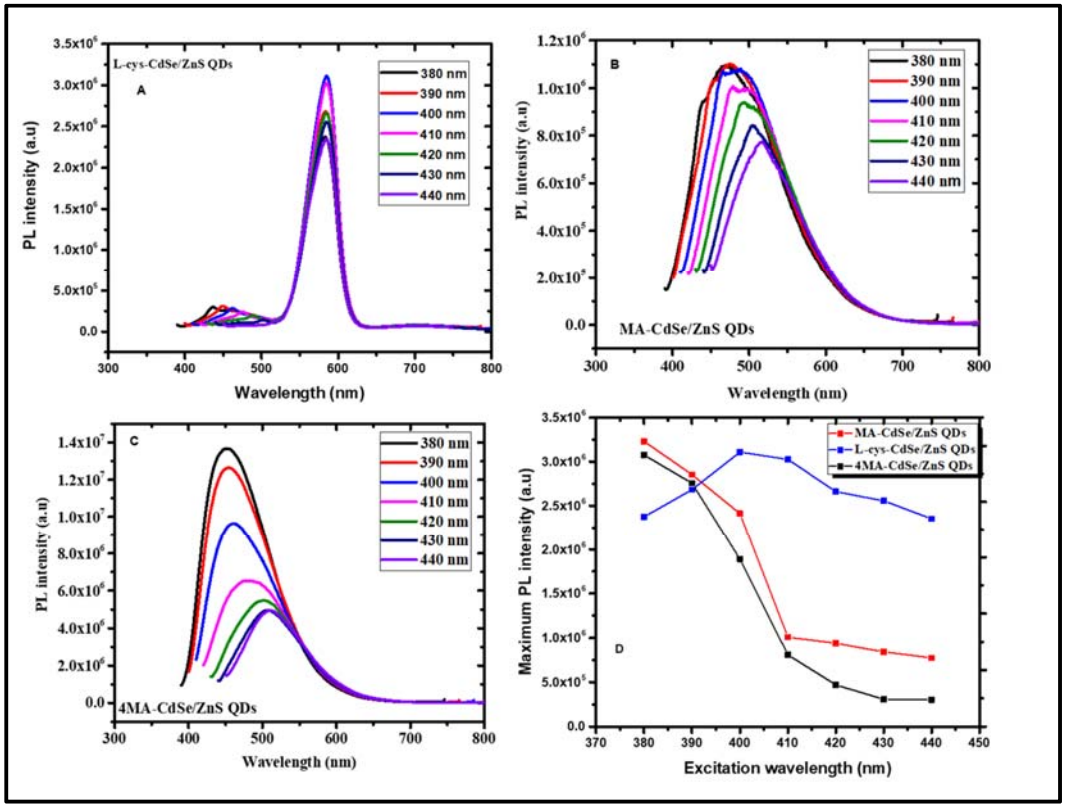

Fig. 6: The effects of excitation wavelengths on the emission spectra of (A) L-cys-CdSe/ZnS QDs, (B) MA-CdSe/ZnS QDs and (C) 4MA-CdSe/ZnS QDs. (D) shows the effect of excitation wavelength on the maximum photoluminescence (PL) intensity of A, B and C.

3.3 Fluorescent properties of CdSe/ZnS QDs, L-cys-CdSe/ZnS QDs, MA-CdSe/ZnS QDs and 4MA-CdSe/ZnS QDs

The fluorescent properties of CdSe/ZnS QDs, L-cys-CdSe/ZnS QDs, MA-CdSe/ZnS QDs and 4MA-CdSe/ZnS QDs were investigated using fluorescence spectrophotometry (**Fig. 7).** Hydrophilic CdSe/ZnS QDs were used in this study in preference to other hydrophilic QDs, such as CsPbX3 QDs, because of their excellent stability. CdSe/ZnS QDs bind capping agents, such as L-cysteine, via ligand exchange. This serves as a stabilizer and refines the surface of CdSe/ZnS QDs, maintaining the PL properties of the QDs. In the case of CsPbX3 QDs, these are made up of an ionic crystal structure and bind capping agents through surface ions. When these surface ions are exposed to water, light and high temperatures, they may degrade which affects the PL properties and stability of the QDs. [30, 31]

The fluorescence emission spectra of CdSe/ZnS QDs and L-cys-CdSe/ZnS QDs prepared in this work were narrow having the same full width at half maximum (FWHM) of 40 nm with maximum emission wavelengths at 560 nm and 584 nm respectively, when excited at 390 nm. The attachment of L-cysteine ligands to the CdSe/ZnS QDs induced a red shift of the emission spectrum with an increase in fluorescence quantum efficiency or quantum yield from 71.2 % of CdSe/ZnS QDs to 89.9 % of L-cys-CdSe/ZnS QDs likely due to surface passivation effects. Upon coupling 1.00 mg and 4.00 mg of MAs to L-cys-CdSe/ZnS QDs, the emission spectra became broader than that of the L-cys-CdSe/ZnS QDs and were slightly blue shifted with the maximum emission wavelength at 474 nm (FWHM=94 nm) and 454 nm (FWHM=81 nm) respectively. The coupling of MAs to L-cys-CdSe/ZnS QDs also caused a decrease in PL quantum yield. This remarkable blue shift and change in quantum yield can be attributed to a change in the surface states of the QDs and is an indication of the successful coupling of MAs to the L-cys-CdSe/ZnS QDs. Despite the emission maxima of these two MA-CdSe/ZnS QDs being broad, and blue shifted, it is notable that they have different emission wavelengths indicating that the amount of MAs used in coupling is responsible for the shift in emission wavelengths. The PL quantum yield, although reduced in the coupled product, was still sufficiently high to be fit for purpose.

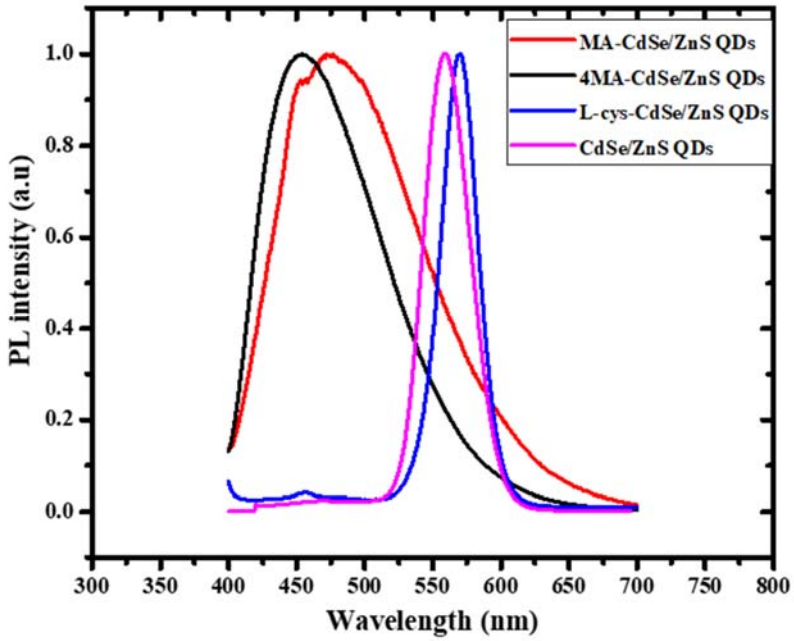

Fig. 7: Normalised PL emission of CdSe/ZnS QDs (dissolved in chloroform), L-cys-CdSe/ZnS QDs, MA-CdSe/ZnS QDs and 4MA-CdSe/ZnS QDs dissolved in water. All samples were excited at 390 nm.

Table 1 Summary of photophysical properties of CdSe/ZnS QDs, L-cys-CdSe/ZnS QDs, MA-CdSe/ZnS QDs and 4MA-CdSe/ZnS QDs

	λ_{em} (nm)	FWHM (nm)	Φ_f (%)
CdSe/ZnS QDs	560	40	71.2
L-cys-CdSe/ZnS QDs	584	40	89.9
MA-CdSe/ZnS QDs	474	94	23.2
4MA-CdSe/ZnS QDs	454	81	22.8

Note: λ_{em} =wavelength at maximum emission, **FWHM** = full width at half maximum, and Φ_f = fluorescence quantum yield.

3.4 FT-IR spectra of L-cys-CdSe/ZnS QDs, MAs, MA-CdSe/ZnS QDs and 4MA-CdSe/ZnS QDs

The FT-IR spectrum of the L-cys-CdSe/ZnS QDs in **Fig. 8** shows characteristic peaks i.e. -N-H, -C-H, and -C=O which confirms their successful functionalization with L-cysteine, while the spectrum for pure MAs shows the expected –C-H and –C=O peaks in addition to the -O-H band. After the coupling of 1.00 mg of MAs to L-cys-CdSe/ZnS QDs, two new bands that can be attributed to -N-C=O modes were observed between 2490 and 2602 cm^{-1}. These peaks in the MA-CdSe/ZnS QD spectrum indicate the presence of amide bonds, which confirms the

successful coupling of MAs to L-cys-CdSe/ZnS QDs. [32, 33] Similar results were observed when 4.00 mg of MAs was used to prepare 4MA-CdSe/ZnS QDs. These results indicate that changing the amount of MAs does not affect the functional groups of the coupled material.

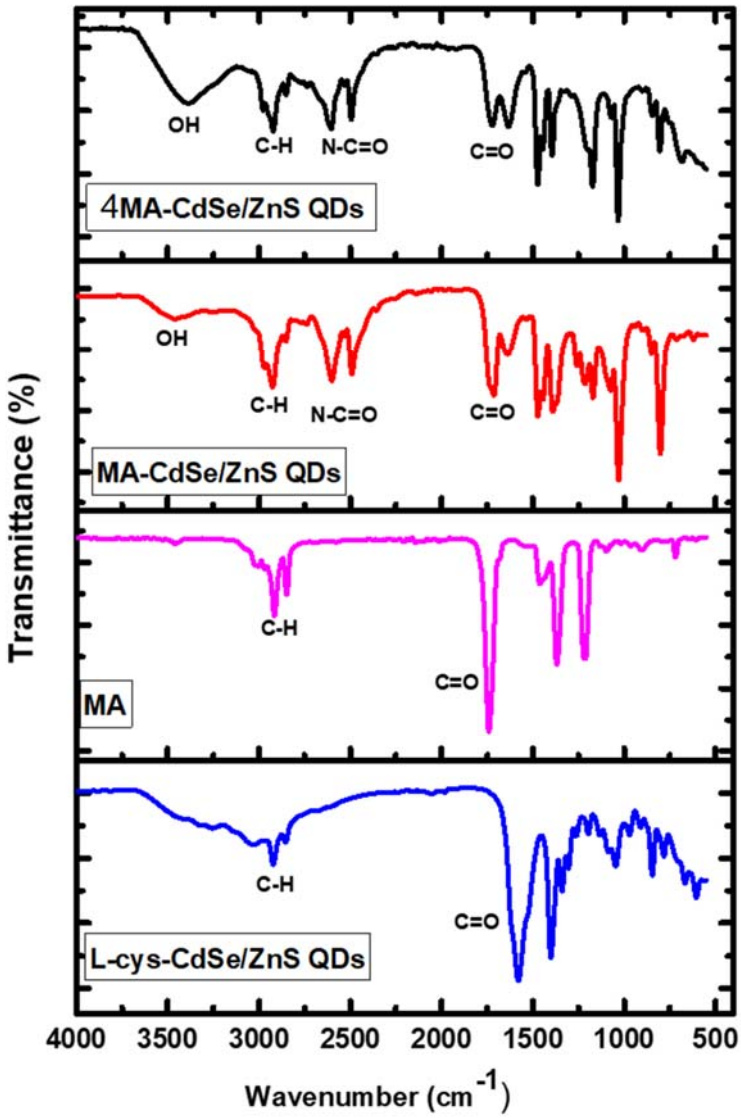

Fig. 8: FT-IR spectra of L-cys-CdSe/ZnS QDs, MAs, MA-CdSe/ZnS QDs and 4MA-CdSe/ZnS QDs analysed in powder form.

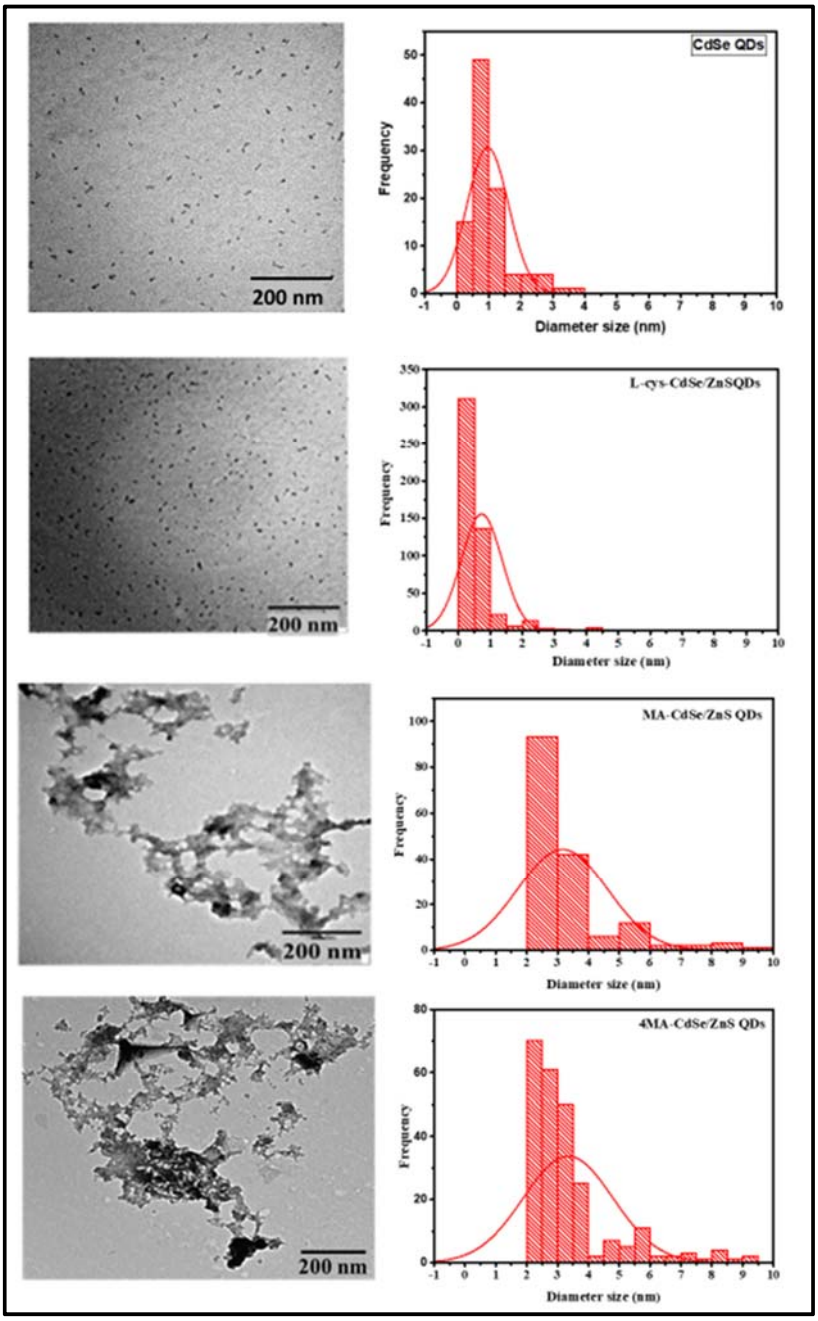

Fig. 9: TEM micrographs of CdSe QDs (dissolved in Chloroform), L-cys-CdSe/ZnS QDs, MA-CdSe/ZnS QDs and 4MA-CdSe/ZnS QDs dissolved in water.

3.5 TEM analysis of CdSe QDs, L-cys-CdSe/ZnS QDs, MA-CdSe/ZnS QDs and 4MA-CdSe/ZnS QDs

The morphology and particle size of CdSe QDs, L-cys-CdSe/ZnS QDs, MA-CdSe/ZnS QDs and 4MA-CdSe/ZnS QDs are shown in **Fig. 9.** It is observed that core CdSe QDs dispersed

well in chloroform while L-cys-CdSe/ZnS QDs dispersed well in water and had an average estimated particle size of 1.0±0.1 nm and 1.0±0.2 nm, respectively. The morphology of MA-CdSe/ZnS QDs and 4MA-CdSe/ZnS QDs show some particle aggregation. The average estimated particle size of MA-CdSe/ZnS QDs was 3.1±0.8 nm, while 4MA-CdSe/ZnS QDs, was 3.3±0.2 nm. This aggregation could be due to the presence of attractive forces between both hydrophilic and hydrophobic groups of the MA-QD particles and this leads to an increase in average particle size of MA-CdSe/ZnS QDs and 4MA-CdSe/ZnS QDs. [34] Changes in the environmental conditions of aggregated particles in porous media slightly affects the size of the coupled material. [34] As a result of this, different average particle sizes were observed when the amount of MAs was increased during the coupling reaction.

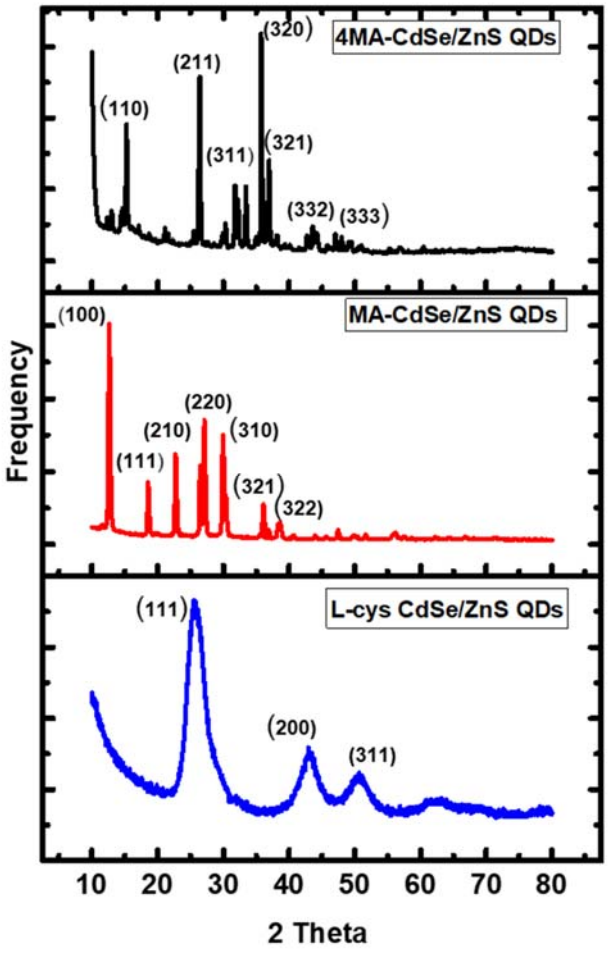

Fig. 10: Powder XRD spectra of L-cys-CdSe/ZnS QDs, MA-CdSe/ZnS QDs and 4MA-CdSe/ZnS QDs.

3.6 Powder XRD analysis of L-cys-CdSe/ZnS QDs, MA-CdSe/ZnS QDs and 4MA-CdSe/ZnS QD

Fig. 10 shows broad peaks for L-cys-CdSe/ZnS QDs at 25.5˚ (111), 43.3˚ (200) and 50.6˚ (311) corresponding to the zinc blende crystal structure as reported previously for this material. [26] MA-CdSe/ZnS QDs have sharper peaks with a significant shift to the left at 7.4° (100), 12.6° (111), 16.4° (210), 20.2° (220), 22.9° (310), 28.2° (321), and 30.0° (322). This shift and the increase in the number of peaks suggests that the coupling of MAs to L-cys-CdSe/ZnS QDs resulted in a change in the crystal phase, which is expected due to the non-crystalline MA moieties present in the MA-CdSe/ZnS QDs. Sharp peak positions of MA-CdSe/ZnS QDs show the crystal structure of the resulting material.

Similarly, sharp peak positions were observed for 4MA-CdSe/ZnS QDs at different positions. The peak positions were at 9.7° (110), 19.7° (211), 23.0° (310), 25.9° (320), 27.9° (321), 35.3° (332) and 38.2° (333). These results suggest that increasing the amount of MAs during the synthesis of MA-CdSe/ZnS QDs slightly changes the crystal structure of the coupled material.

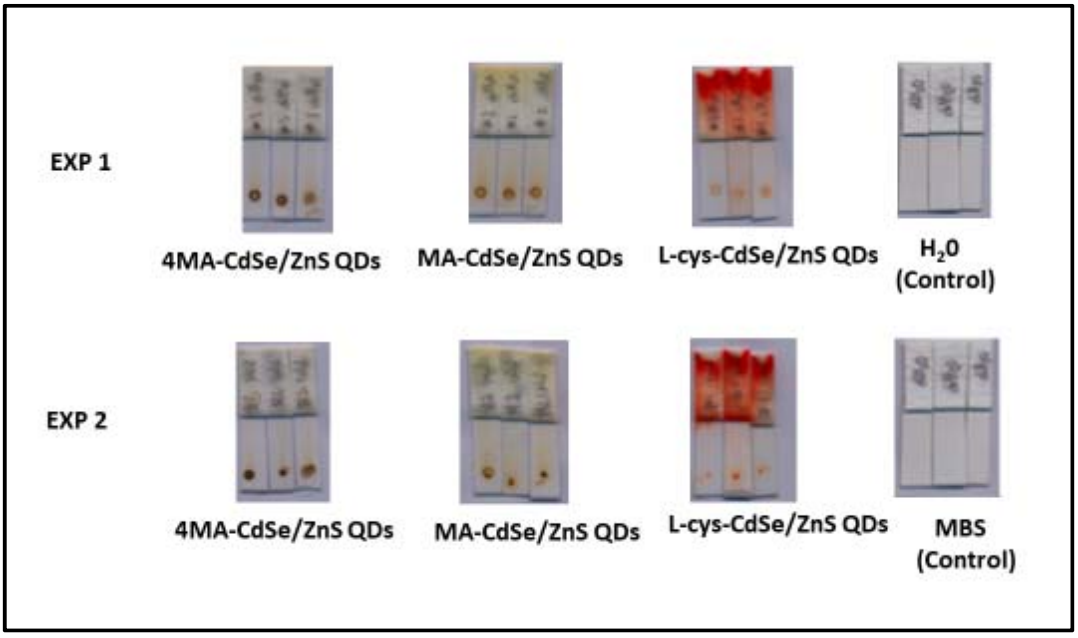

Fig.11: Images of the strips of nitrocellulose membrane taken after each of the two lateral flow experiments of L-cys-CdSe/ZnS QDs, MA-CdSe/ZnS QDs and 4MA-CdSe/ZnS QDs with water (experiment 1) and membrane blocking solution (MBS) (experiment 2) as eluents.

3.7 Paper-based lateral flow of L-cys-CdSe/ZnS QDs, MA-CdSe/ZnS QDs and 4MA-CdSe/ZnS QDs

Paper-based lateral flow tests for L-cys-CdSe/ZnS QDs, MA-CdSe/ZnS QDs and 4MA-CdSe/ZnS QDs were conducted to investigate their potential application in TB detection and diagnosis. **Fig.11** shows that L-cys-CdSe/ZnS QDs, MA-CdSe/ZnS QDs and 4MA-CdSe/ZnS QDs were able to visually flow through the strips of nitrocellulose membrane in both eluents, that is water and membrane blocking solution. Membrane blocking solution is a buffer solution used to block nonspecific sites on the nitrocellulose membrane and made up of 0.1% proclin, water, bovine serum albumin (BSA), goat IgG and Tween® 20. The rate flow of the fluorophores through the strips of nitrocellulose membrane was fast enough to be seen with the naked eye.

4. Conclusion

Water-soluble core/shell CdSe/ZnS QDs capped with L-cysteine were successfully synthesised and coupled to MAs to form MA-CdSe/ZnS QDs with potential prospects as a water-soluble fluorescent TB probe. The coupled MA-CdSe/ZnS QDs and synthesized L-cys-CdSe/ZnS QDs were characterized by absorption and fluorescence spectroscopy, TEM analysis, FT-IR and XRD spectroscopy. The absorption results indicated that both CdSe/ZnS QDs and MA-CdSe/ZnS QDs show broad absorption bands ranging from 200 to 420 nm which allows for variation of excitation wavelengths in fluorescence sensing applications. It is also noted that the amount of MAs in the coupled material affected the emission wavelength thereof. Fluorescence results showed that CdSe/ZnS QDs and L-cys-CdSe/ZnS QDs had narrow emission spectra with maximum emission wavelengths at 560 nm and 584 nm, when exciting at 390 nm, while MA-CdSe/ZnS QDs and 4MA-CdSe/ZnS QDs had broader spectra with a maximum emission at 474 nm and at 454 nm, respectively. The presence of -N-C=O peaks in MA-CdSe/ZnS QDs and 4MA-CdSe/ZnS QDs FT-IR spectra indicated the presence of amide bonds, which confirms the successful coupling of MAs to L-cys-CdSe/ZnS QDs. TEM analysis results showed average estimated size particle distribution of CdSe QDs to be 1.0±0.1 nm, 1.0±0.2 nm for L-cys-CdSe/ZnS QDs, 3.1±0.8 nm for MA-CdSe/ZnS QDs and 3.3±0.2 nm for 4MA-CdSe/ZnS QDs. The powder XRD results showed a shift and an increase in the number of peaks for MA-CdSe/ZnS QDs and 4MA-CdSe/ZnS QDs relative to the L-cys-CdSe/ZnS QDs. This suggests that the coupling of MAs to L-cys-CdSe/ZnS QDs changed the crystal structure of the MA-CdSe/ZnS QDs. Sharp peak positions observed in MA-CdSe/ZnS QDs

and 4MA-CdSe/ZnS QDs confirms that changing the amount of MAs does not negatively affect the crystallinity of the material, but the crystal structure did change from the zinc blende of the uncoupled QDs. Paper-based lateral-flow experiments confirmed visually the flow of L-cys-CdSe/ZnS QDs, MA-CdSe/ZnS QDs and 4MA-CdSe/ZnS QDs through the nitrocellulose membrane with water and membrane blocking solution as eluents. Due to their good solubility in water (0.1 mg/ml), and high fluorescence, MA-QDs have the potential to be used as a point of care fluorescent probe for the lateral flow detection of antibodies and the diagnosis of tuberculosis.

Acknowledgements

TWAS-NRF doctoral scholarship funding and a University of Pretoria postgraduate student bursary is gratefully acknowledged (KK). The Next Generation Health unit of the CSIR, specifically Alma Truyts, is acknowledged for assisting with lateral flow experiments and the Microscopy and Microanalysis Laboratory of the University of Pretoria for assistance with microscopy measurements.

References

[1] N. Fogel, *Tuberculosis* 2015, 95, 527.

[2] T.R. Lerner, S. Borel, D.J. Greenwood, U. Repnik, M.R. Russell, S. Herbst, M.L. Jones, L.M. Collinson, G. Griffiths, M.G. Gutierrez, *J. Cell Biol.* 2017, 216, 583.

[3] A. Welin, J. Raffetseder, D. Eklund, O. Stendahl, M. Lerm, *J. Innate Immun.* 2011, 3, 508.

[4] D.R. Silva, F.C.d.Q. Mello, G.B. Migliori, *J. Bras Pneumol.* 2020, 46, 1806.

[5] S. Sudha, *Int. J. Med. Eng. Inform.* 2016, 8, 27.

[6] T.R. Frieden, T.R. Sterling, S.S. Munsiff, C.J. Watt, C. Dye, *The Lancet* 2003, 362, 887.

[7] J. Peter, C. Green, M. Hoelscher, P. Mwaba, A. Zumla, K. Dheda, *Curr. Opin. Pulm. Med.* 2010, 16, 262.

[8] S.T. Thanyani, V. Roberts, D.G.R. Siko, P. Vrey, J.A. Verschoor, *J. Immunol. Methods* 2008, 332, 61.

[9] M.S. Verma, J.L. Rogowski, L. Jones, F.X. Gu, *Biotechnol. Adv.* 2015, 33, 666.

[10] A. Mansour, S. Tammam, A. Althani, H.M.E. Azzazy, *J. Microbiol. Methods* 2017, 139, 165.

[11] E.J. North, M. Jackson, R.E. Lee, *Curr. Pharm. Des.* 2014, 20, 4357.

[12] M. Watanabe, Y. Aoyagi, M. Ridell, D.E. Minnikin, *Microbiology* 2001, 147, 1825.

[13] F.L. Ndlandla, V. Ejoh, A.C. Stoltz, B. Naicker, A.D. Cromarty, S. van Wyngaardt, M. Khati, L.S. Rotherham, Y. Lemmer, J. Niebuhr, C.R. Baumeister, J.R. Al Dulayymi, H. Swai, M.S. Baird, J.A. Verschoor, *J. Immunol. Methods* 2016, 435, 50.
[14] S. Shang, D. Kats, L. Cao, E. Morgun, D. Velluto, Y. He, Q. Xu, C.-R. Wang, E.A. Scott, *Front. Immunol.* 2018, 9, 2709.
[15] J. Verschoor, *Trop. Med. Int. Health* 2010, 15, 1360.
[16] J.A. Verschoor, C. Baumeister, A method of diagnosing tuberculosis, *Google Patents*, 2016.
[17] J.A. Verschoor, I.E. OKEKE, L. Kalombo, Y. Lemmer, Core elements for point of care diagnosis of tuberculosis, *Google Patents*, 2017.
[18] A. Cheepsattayakorn, R. Cheepsattayakorn, *J. Nanotech. Diagn. Treat.* 2013, 1, 19.
[19] O. Adegoke, T. Nyokong, P.B. Forbes, *J. Alloys Compd.* 2015, 645, 443.
[20] O. Adegoke, P. Mashazi, T. Nyokong, P.B. Forbes, *Opt. Mater.* 2016, 54, 104.
[21] I. Martynenko, A. Litvin, F. Purcell-Milton, A. Baranov, A. Fedorov, Y. Gun'ko, *J. Mater. Chem. B* 2017, 5, 6701.
[22] E.B. Bahadır, M.K. Sezgintürk, *TrAC-Trends Anal. Chem.* 2016, 82, 286.
[23] L. Anfossi, F. Di Nardo, S. Cavalera, C. Giovannoli, G. Spano, E.S. Speranskaya, I.Y. Goryacheva, C. Baggiani, *Mikrochim. Acta* 2018, 185, 94.
[24] M. Sajid, A.-N. Kawde, M. Daud, *J. Saudi Chem. Soc.* 2015, 19, 689.
[25] H. Ranchod, F. Ndlandla, Y. Lemmer, M. Beukes, J. Niebuhr, J. Al-Dulayymi, S. Wemmer, J. Fehrsen, M. Baird, J. Verschoor, *PloS one* 2018, 13, e0200298.
[26] H. Montaseri, P.B. Forbes, *Mater.Today Commun.* 2018, 17, 480.
[27] O. Adegoke, H. Montaseri, S.A. Nsibande, P.B.C. Forbes, *J. Alloys Compd.* 2017, 720, 70.
[28] Y. Chen, W. Xing, Y. Liu, X. Zhang, Y. Xie, C. Shen, J.G. Liu, C. Geng, S. Xu, *Nanomaterials* 2020, 10, 317.
[29] D. Magde, R. Wong, P.G. Seybold, *Photochem. Photobiol* 2002, 75, 327.
[30] Y. Zhao, C. Xie, X. Zhang, P. Yang, *ACS Appl. Nano Mater* 2021, 4, 5478.
[31] W. Shi, X. Zhang, H.S. Chen, K. Matras-Postolek, P. Yang, *J. Mater. Chem. C.* 2021, 9, 5732.
[32] Y. Zhang, Y. Sun, T. Wang, J. Liu, B. Spingler, S. Duttwyler, *Molecules* 2018, 23, 3137.
[33] L.H. Chan-Chan, G. González-García, R.F. Vargas-Coronado, J.M. Cervantes-Uc, F. Hernández-Sánchez, A. Marcos-Fernandez, J.V. Cauich-Rodríguez, *Eur. Polym. J.* 2017, 92, 27.

[34] P. Babakhani, *Sci. Rep.* 2019, 9, 1.